New recommended ωγ for the E_{r}^{c.m.}=458 keV resonance in ^{22}Ne(p,γ)^{23}Na

K. J. Kelly, A. E. Champagne, R. Longland, and M. Q. Buckner

Phys. Rev. C **92**, 035805 — Published 4 September 2015

DOI: 10.1103/PhysRevC.92.035805

New Recommended $\omega\gamma$ for the E_r^{cm} = 458 keV Resonance in ^{22}Ne(p,γ)^{23}Na

K. J. Kelly[1,3], A. E. Champagne[1,3], R. Longland[2,3], and M. Q. Buckner[1,3]
[1] *Department of Physics and Astronomy, University of North Carolina at Chapel Hill, Chapel Hill, NC 27599-3255, USA*
[2] *Department of Physics and Astronomy, North Carolina State University, Raleigh, NC, 27695, USA and*
[3] *Triangle Universities Nuclear Laboratories, Duke University, Durham, NC 27708-0308, USA*
(Dated: August 14, 2015)

The E_r^{cm} = 458 keV resonance in ^{22}Ne(p,γ)^{23}Na is an ideal reference resonance for measurements of cross sections and resonance strengths in noble gas targets. We report on a new measurement of the strength of this resonance. Data analysis employed the TFractionFitter class of ROOT combined with GEANT simulations of potential decay cascades from this resonance. This approach allowed us to extract precise primary branching ratios for decays from the resonant state, including a new primary branch to the 7082-keV state in ^{23}Na. Our new resonance strength of $\omega\gamma$(458 keV) = 0.583(43) eV is more than 1-σ higher than a recent high-precision result that relied on literature branching ratios.

PACS numbers: 25.40.Lw,26.20.Cd,27.30.+t

I. INTRODUCTION

Measurements of weak resonant or direct-capture reactions often use the strengths of well-known resonances as a "standard" from which the absolute cross-section scale can be determined. The E_r^{cm} = 458 keV resonance in the ^{22}Ne(p,γ)^{23}Na reaction (E_x = 9252.1 keV, S_p = 8794.11(2) keV [1]) is an ideal standard resonance for noble gas targets. Such a reference is important because of interest in the reactions that produce and destroy sodium in massive asymptotic giant branch stars. The sodium abundance is governed by the ^{20}Ne(p,γ)^{21}Na, ^{22}Ne(p,γ)^{23}Na, and ^{23}Na(p,γ)^{24}Mg reactions, all of which have significant uncertainties at the energies of interest [2]. An improved determination of $\omega\gamma$(458 keV) will thus facilitate more accurate measurements of the first two reactions.

The strength of this resonance has been reported multiple times in the literature [3–5], including the recent, high-precision measurement by Ref. [6]. This measurement relied on literature branching ratios, sources for which are limited to the results of Refs. [3, 4], which were reported without uncertainties. In particular, Ref. [6] adopted a ground-state branching ratio of B(R→0)= 0.465(23), deduced from a weighted average of the values reported in Refs. [3, 4] and their resulting resonance strength was inversely proportional to this branching ratio. In this work we report on a new measurement of branching ratios for the decay of the 458-keV resonance and use this information to determine a revised resonance strength. Changes from the previously accepted values include a newly discovered branch to the 7082-keV state in ^{23}Na as well as a decrease of approximately 10% in the ground state branching ratio used in Ref. [6]. These results were obtained using GEANT version 4.9.6 [7] simulations of potential decay cascades from the 9252-keV resonant state in ^{23}Na combined with a fit to the measured γ-ray spectrum determined using the TFractionFitter [8] class of ROOT [9]. The overall impact of these new branching ratios is an increase in the resonance strength of Ref. [6] by 11.3% (or about 1.2 σ). This increase extends to all higher-lying resonances in the ^{22}Ne(p,γ)^{23}Na reaction.

II. EXPERIMENTAL PROCEDURE

Data for this work were taken with the 1-MV JN van de Graaff accelerator at the Laboratory for Experimental Nuclear Astrophysics (LENA) [10], located at the Triangle Universities Nuclear Laboratory (TUNL). The JN accelerator can provide proton beams in the energy range of $\sim$ 200 keV – 1 MeV, with a maximum intensity of about 120 μA and a typical energy spread of 1–3 keV. The energy calibration was established to <1 keV by using well-known resonances of the reactions ^{18}O(p,γ)^{19}F, ^{26}Mg(p,γ)^{27}Al, and ^{27}Al(p,γ)^{28}Si [10].

A target of ^{22}Ne implanted into a tantalum target backing was fabricated using the Eaton Ion Implanter located at the University of North Carolina at Chapel Hill. An ion implantation energy of 100 keV was used, yielding a target thickness of approximately 20 keV at the resonance energy. The ^{22}Ne:Ta stoichiometry of the target used for this work was measured to be approximately 1:4 using the 458-keV resonance in ^{22}Ne(p,γ)^{23}Na. The proton beam entered the target chamber through a copper tube, extending to less than 1 cm from the surface of the target. The copper tube was cooled by a LN_2 reservoir to trap potential target contaminants. To minimize target degradation from beam heating, the target was cooled using chilled, deionized water and the beam was rastered into a beamspot $\sim$ 12 mm in diameter. In order to suppress the emission of secondary electrons from the target, permanent magnets were positioned at the end of the tube along with an electrode biased to -300 V. This formed a Faraday cup for measuring beam current. Total beam charge accumulated on target amounted to $\sim$ 0.01 C. The yield on the 458-keV resonance in ^{22}Ne(p,γ)^{23}Na was measured before and after data acquisition to ensure that the target did not degrade.

Data were collected with a 135% coaxial HPGe detector placed 1.1 cm from the target. A laboratory energy of E_p = 494 keV was used, which was slightly above the maximum yield of the resonance, and beam currents were held to $\approx$ 4 μA. Both of these experimental parameters were intended to keep the dead time to below 5%. The resonance strength reported in this work depends only on the results of Ref. [6] and the primary branching ratios reported in Sec. III, which are independent of the beam energy offset from the maximum resonance yield. The HPGe detector has been thoroughly characterized through extensive simulation studies using GEANT (version 4.9.6) and measurements of both radioactive sources, such as ^{56}Co, ^{22}Na, ^{54}Mn, ^{137}Cs, and ^{60}Co, and of the ^{14}N(p,γ)^{15}O, ^{18}O(p,γ)^{19}F, ^{23}Na(p,γ)^{24}Mg, and ^{27}Al(p,γ)^{28}Si reactions[2, 11–13]. The critical dimensions used in the simulations were obtained from a CT scan of the detector [14].

III. DATA ANALYSIS AND RESULTS

The traditional means of analyzing γ-ray spectra involves integrating photopeaks corresponding to transitions of interest. Along with external backgrounds, escape peaks and Compton events associated with these transitions are treated as backgrounds that could obscure weak transitions. However, the majority of events detected reside in the Compton continuum and could in principle be used to extract decay strengths, provided that the response of the detector can be accurately measured or simulated. This approach uses the TFractionFitter [8] class of ROOT [9] and was recently applied to HPGe spectra in Refs. [15, 16]. A similar technique was also applied to NaI spectra in Ref. [17]. The notation in the following description varies slightly from Ref. [15] to improve consistency with the original work by Ref. [8]. A complete, detailed description of this data analysis method will be provided in a forthcoming publication [18], which shall serve as the primary reference for this analysis method.

Individual GEANT [7] simulations were generated for each possible nuclear decay cascade from the 9252-keV state in ^{23}Na populated by the 458-keV resonance in ^{22}Ne(p,γ)^{23}Na. Every GEANT simulation used in this work was calculated with version 4.9.6. All secondary decays from lower lying excited states in ^{23}Na were included in each decay cascade template using the branching ratios listed in Ref. [1]. Given that the resonance spin is $J_R = 1/2$, transitions to all lower lying excited states with $J = 1/2$, $3/2$, or $5/2$ were considered here, but only those with a non-zero contribution were kept for the final fit to the data. In this manner, we could potentially identify transitions that escaped prior detection. This resonance spin also implies that all primary γ-rays are emitted isotropically. Angular distributions and direction-direction correlations for all secondary γ-rays were calculated according to Ref. [19] using the level spin assignments of Ref. [1] and were included in all simulations used here. A rigorous investigation of the agreement between simulated and experimental spectra in regards to the the shape, magnitude, and position of each γ-ray peak was carried out in order to obtain an accurate simulation of the experimental data.

Each simulation was then used as a "template" for a fit to the experimental data spectrum. The fit also included simulations of beam induced backgrounds, such as those arising from the ^{12}C(p,γ)^{13}N and ^{11}B(p,γ)^{12}C reactions, as well as the measured room and cosmic-ray background. The TFractionFitter [8] class of ROOT [9] was used to vary the intensity of each template within each bin to obtain a maximum likelihood fit to the data. In the following, we summarize the discussion of this technique found in Ref. [8]. If we assume that every spectrum has n bins, indexed by i, and that the fit includes m templates, indexed by j, then the likelihood function that was maximized is given by

$$\ln(\mathscr{L}) = \left[\sum_{i=1}^{n} d_i \ln f_i - f_i\right] + \left[\sum_{i=1}^{n}\sum_{j=1}^{m} a_{ji} \ln A_{ji} - A_{ji}\right], \tag{1}$$

where $\mathscr{L}$ is the likelihood, d_i and a_{ji} are the counts in bin i from the data and from template j, respectively, and the parameter A_{ji} is the predicted number of counts in bin i from template j. The parameter f_i is the predicted number of counts in bin i from the fit to the data, given by

$$f_i = \sum_{j=1}^{m} p_j A_{ji}. \tag{2}$$

The parameters p_j are defined by

$$p_j = \frac{A_{total}^{data}}{A_j^{sim}} F_j, \tag{3}$$

where A_{total}^{data} and A_j^{sim} are the total area of the data spectrum and of template j, respectively. The F_j are the fractions of A_{total}^{data} accounted for by a particular template as determined by the fitting procedure. Note that the F_j sum to 1. The goal is to determine the F_j or, equivalently, the p_j.

The first term in the likelihood function described by Eq. 1 takes into account the random, statistical nature of experimental data. This term alone is used in the common "binned maximum likelihood" fit. The second term takes into account the fact that Monte Carlo generated template histograms also display similar random, statistical fluctuations and is essential when determining a maximum likelihood fit using Monte Carlo input.

By defining the parameters t_i such that

$$t_i = 1 - \frac{d_i}{f_i} \quad \& \quad A_{ji} = \frac{a_{ji}}{1 + p_j t_i}. \tag{4}$$

Equations 2 and 4 can be used to derive the relation

$$f_i = \frac{d_i}{1-t_i} = \sum_{j=1}^{m} \frac{p_j a_{ji}}{1+p_j a_{ji}}, \quad (5)$$

which can be rewritten as

$$\sum_{j=1}^{m} \frac{p_j a_{ji}}{1+p_j a_{ji}} - \frac{d_i}{1-t_i} = 0. \quad (6)$$

Assuming a set of p_j values, Eq. 6 was used to iteratively solve for the n parameters, t_i, via the Newton-Raphson method. Once a set of t_i values was established, the MINUIT package [20] was used to determine new values for each p_j value in this iterative calculation for a maximum of Eq. 1. Iterations of Eqs. 1 and 6 continued until a satisfactory numerical precision was reached for the final set of p_j values, thereby yielding the desired quantities, F_j.

The branching ratios were determined not by F_j, but by the ratio

$$\mathrm{B(R} \rightarrow E_j) = N_j^{data}/N_R^{data}, \quad (7)$$

where the primary decay transition described by template j is initiated via a primary decay from R, the resonant state, to the state in ^{23}Na with energy E_j. The quantity N_j^{data} is the number of resonant excitations produced in the target that decay through cascade j (or equivalently, the partial number of reactions corresponding to a particular decay cascade) and N_R^{data} is the total number of resonant excitations observed in the data. The quantity N_j^{data} can be obtained from N_j^{sim}, the number of simulated excitations for cascade j, and F_j via Ref. [15], Eq. 3.

$$N_j^{data} = \frac{A_{total}^{data}}{A_j^{sim}} F_j N_j^{sim}, \quad (8)$$

where A_j^{sim} is the total number of counts in simulated spectrum of cascade j and A_{total}^{data} is the same quantity for the measured spectrum. Finally, N_R^{data} can be obtained from

$$N_R^{data} = \sum_{j=1}^{m} N_j^{data}. \quad (9)$$

There is no need to subtract background since the F_j take the background template into account. Also, coincidence summing is automatically included in the GEANT simulations, obviating the need for summing corrections. In general, N_R^{data} can then be used to derive the resonance strength (in the case of a resonant reaction), or the cross section (in the case of a non-resonant reaction). By analyzing data in this manner, the statistics of the *entire* spectrum were considered. This is a significant advantage as, for example, the simulated 458-keV ^{22}Ne(p,γ)^{23}Na resonance ground-state photopeak is only $\sim$5% of the whole simulated spectrum.

The ^{22}Ne(p,γ)^{23}Na data spectrum used in this work is shown in Fig. 1 along with the final fit to the data and selected templates from which the fit was determined. The data are shown in black with the fit in green. The room background template is shown in red and the two strongest resonant state decay templates are shown in blue. All resonance primary peaks are indicated with blue arrows. A total of 15 templates were used during the final minimization process, translating to 15 total simultaneously fit p_j values. These correspond to the room background template, 4 beam-induced background templates, and 10 resonant decay templates. Although the R$\rightarrow$3848 transition is allowed on the basis of spin considerations, there was no evidence in the data for this transition and since the fit would not converge with this template included, this transition was not considered during the fitting procedure.

The resulting branching ratios are shown in Tab. I along with those reported previously in Refs. [3, 4]. By not limiting our analysis to only the decays already known in the literature, it was possible to detect a new decay branch to the 7082-keV state in ^{23}Na. The existence of this transition is verified in Fig. 2 through a comparison of the measured yield across the 458-keV resonance of the 2170-keV primary γ-ray emitted during the R$\rightarrow$7082 transition to that of the well-known 6270-keV γ-ray emitted during the R$\rightarrow$2982 transition. Black circles and red diamonds show the 6270 and 2170-keV γ-ray yields, respectively. The yield scale for red or black data points is indicated by the y-axis of the same color. The shape and position of the 6270-keV γ-ray yield curve is reproduced by that of the 2170-keV γ-ray. All other γ-rays analyzed in this work have been reported previously in Refs. [3, 4] and correspond to known decays from the resonant state.

Beyond this, the most notable difference between the present results and those of Refs. [3, 4] is the decrease in the R$\rightarrow$0 branching ratio by approximately 10–13%. This is the strongest of transition from the 9252-keV state and is also the branch used in the high-precision $\omega\gamma$(458 keV) measurement of Ref. [6]. In that work, their calculated $\omega\gamma$(458 keV) was inversely proportional to B(R$\rightarrow$0); a 10% decrease in B(R$\rightarrow$0) induces an approximately 11.3% change in their $\omega\gamma$(458 keV). Additionally, the technique used by Longland et al. [6] was independent of systematic effects associated with target stoichiometry, charge integration, or absolute detector efficiency. For this reason, we have chosen to correct their result by replacing their assumed ground-state transition branching ratio with our present measurement. Thus, we recommend $\omega\gamma$(458 keV) = 0.583(43) eV. The percent uncertainty in this resonance strength has also been reduced from 9.7% in Longland et al. [6] to 7.3% uncertainty reported here. It should be noted that this resonance strength is indeed consistent with our measured yield and assumed stoichiometry.

IV. VALIDATION OF THE TECHNIQUE AND COMPARISON WITH PREVIOUS RESULTS

A. Experimental Yield Calculations

Our technique can be tested by extracting experimental yields in the traditional fashion of integrating photopeaks corresponding to the individual primary transitions. The total yield of the reaction as determined from the strength of a particular primary transition, j, assuming a certain set of branching ratios, k, can be written as [19]:

$$Y_{j,k} = \frac{1}{N_B}\left\{\frac{N_\gamma}{\eta_p W}\left[\frac{f_{SC}}{B}\right]_k\right\}_j , \qquad (10)$$

where N_B is the total number of bombarding particles and N_γ is the peak intensity of a primary γ-ray of interest. The parameters B and η_p are the branching ratio and full-energy peak efficiency, respectively, while W describes the angular distribution of the γ-ray being analyzed. The quantity f_{SC} is a γ-ray intensity correction factor that takes coincidence-summing effects into account. This factor includes the effects of direction-direction correlations between γ-rays and is expanded upon in Sec. IV B. With the exception of N_B, all of these quantities are specific to the particular transition, j, and only f_{SC} and B are specific to the chosen branching ratio set, k. However, $Y_{j,k}$ should be independent of the primary transition photopeak being analyzed. In other words, if the relative branching ratios of the set k are correct, then the experimental photopeak analysis of each primary transition j should result in the same $Y_{j,k}$ and be mutually consistent. Therefore, we chose to probe the accuracy of the present branching ratios as well as those of of Piiparinen et al. [3] and Meyer et al. [4] by analyzing the consistency of $Y_{j,k}$ as calculated for every observed primary transition. Changes in the calculated $Y_{j,k}$ are almost entirely the result of changes between the present branching ratios and those of Refs. [3] and [4].

The angular distribution factor, W, was equal to 1 for every primary transition because the 9252-keV resonant state in ^{23}Na excited by this $E_r^{cm} = 458$ keV resonance has spin $J_R = 1/2$. The quantity N_B was equal to ~ 0.01 C for every $Y_{j,k}$ calculation. The photopeak intensity, N_γ, was different for each primary γ-ray, but remained constant with respect to the branching ratio set being analyzed. GEANT simulations of the Ge detector used in this work have been shown to reproduce experimental full-energy peak efficiencies to within 3-5% [2, 11–13]. Therefore, simulated η_p values at the primary γ-ray energies using mono-energetic GEANT simulations of the detector geometry were used in Eq. 10.

B. Coincidence-Summing Corrections

Experimental γ-ray spectra can be significantly altered by coincidence-summing effects when a close source-detector geometry is used. This is a common problem in measurements of small cross sections relevant to nuclear astrophysics. The coincidence-summing correction factor, f_{SC}, was used to correct for this effect. To be clear, f_{SC} is not used to correct photopeak intensities for random pulse pileup summing which occurs when γ-rays from different decay cascades are incident upon the detector within a narrow time window [21]. Instead, f_{SC} is used to correct data for events when two or more γ-rays from the *same* decay cascade are incident upon the detector. This can result in a signal corresponding to the sum of the energy deposited by each individual γ-ray. If, for example, all incident γ-rays deposit all of their energy within the detector, an effect referred to as "summing-in" occurs in which a signal corresponding to the ground-state transition energy is produced and the net photopeak intensities of the incident γ-rays are reduced by one count each. If, on the other hand, a full energy deposition of one γ-ray is coincident with a partial energy deposition of another, then "summing-out" occurs in which the net photopeak intensity of the first γ-ray is reduced by one count. Note that direction-direction correlations between γ-rays influence coincidence summing.

In this work a newly developed method of correcting experimental data for coincidence-summing effects was used. Other methods exist and are summarized in Ref. [22]. These can be categorized as follows: dedicated computer codes, most of which require input of full-energy peak and total efficiency data [23–30], recursive algorithms coupled to Monte Carlo simulations for efficiencies [31], recursive matrix based calculations with practical approaches for efficiencies [32], and full Monte Carlo simulations with MCNP, GEANT3.21, and GEANT4 [7, 33, 34]. In nuclear astrophysics the methods of Ref. [35] have been used to correct data for coincidence-summing effects [11, 12, 36]. Additionally, expressions from Ref. [21] describing detector efficiency as a function of γ-ray energy and of the distance from the source to the detector combined with "the GEANT4 routine" have been applied to nuclear astrophysics data in previous reaction measurements [37, 38].

GEANT simulations naturally include coincidence summing. However, the method used here deconstructs the GEANT output into contributions to the simulated spectrum from each individual photon incident upon a sensitive detector region. This is accomplished by filtering the GEANT output according to the information about each hit in a sensitive detector provided by the GEANT framework. In particular, the parent, particle, and process ID numbers, the time, energy deposition, and position associated with each hit, and the creation and momentum direction of particles involved in each hit are required for this sum correction method. When these parameters are used to filter GEANT simulation data in the proper manner, the energy deposition attributed to each individual photon can be determined and recorded in a secondary simulation spectrum. This spectrum is *free* of coincidence-summing effects. The f_{SC} factors can then

be calculated according to

$$f_{SC} = N_{\gamma,SC}/N_{\gamma,NSC} \quad (11)$$

where $N_{\gamma,SC}$ and $N_{\gamma,NSC}$ are the simulated photopeak intensities from the spectrum that is sum corrected (SC) and from the spectrum that is not sum corrected (NSC), respectively.

Note that input of full-energy peak or total efficiencies or Q solid angle attenuation coefficients [19] are not required for this sum correction method. The effects of these parameters are taken into account during simulation runtime. This method also provides the user with an entire sum-corrected spectrum that could in principle be used, for example, to correct escape peaks or other regions of the spectrum between photopeaks for coincidence-summing effects. This sum-corrected spectrum differs from a simulation spectrum created from the combination of multiple mono-energetic GEANT simulations in that direction-direction correlations between γ-rays can be taken into account. Data validating this sum correction method can be found in the Appendix. Full simulations of the the 458-keV resonance in the ^{22}Ne(p,γ)^{23}Na reaction were calculated using the present branching ratios as well as those of Refs. [3] and [4] for this work. These simulations were corrected for coincidence-summing effects according to the method described above and used to extract f_{SC} factors according to Eq. 11 for all primary γ-rays. This allowed each calculated value of $Y_{j,k}$ to include a uniquely calculated f_{SC} value according to the primary γ-ray transition and branching ratio set being analyzed.

C. Results

The parameters N_B, η_p, and f_{SC} were assumed to each have a 3% uncertainty for all calculations. Branching ratios were assumed to have a 5% uncertainty for calculations using the results of Refs. [3] and [4]. Uncertainties in the present branching ratios are listed in Tab. I. Uncertainties in N_γ values were calculated from the experimental spectrum, taking the nearby background into account, and were statistical in nature.

The results of these experimental yield calculations are shown in Fig. 3. The dashed line at $Y_{j,k} = 1$ is shown to help guide the eye. The two dashed lines above and below $Y_{j,k} = 1$ represent a factor of 2 and 3 deviation from $Y_{j,k} = 1$. Yields as calculated using the present branching ratios are shown as blue diamonds while the results using the branching ratios of Piiparinen et al. [3] and Meyer et al. [4] are shown as red squares and open circles, respectively. Note that the R→3848 transition reported in Ref. [3] was not observed in this work. As such, the N_γ used for that experimental yield calculation at the 5404-keV γ-ray energy corresponding to this transition is consistent with the observed background level in that region of our data spectrum.

The geometric standard deviation of the set of experimental yields calculated using the branching ratio set k, σ_k^{geo}, is given by

$$\sigma_k^{geo} = exp\left\{\left[\frac{1}{N}\sum_j^N \ln\left(\frac{Y_{j,k}}{\mu_k^{geo}}\right)^2\right]^{\frac{1}{2}}\right\}, \quad (12)$$

where the μ_k^{geo} is the geometric mean and N is the total number of transitions considered in a particular data set. This quantity was calculated with each set of $Y_{j,k}$ values to characterize the consistency of each data set. The geometric standard deviations of the $Y_{j,k}$ calculated using the branching ratios of Piiparinen et al. [3] and Meyer et al. [4], $\sigma^{geo}_{Piiparinen(1971)} = 1.93$ and $\sigma^{geo}_{Meyer(1973)} = 1.46$, are 77% and 34% higher than that of the $Y_{j,k}$ calculated using the present branching ratios, $\sigma^{geo}_{present} = 1.09$. Additionally, the new branch to the 7082-keV state in ^{23}Na reported in the present branching ratio set, corresponding to a primary γ-ray energy of 2170-keV, is internally consistent with the other transitions that we have detected and which were were seen previously.

Finally, it is important to note that the $Y_{j,k}$ determined from the ground-state transition γ-ray peak on the arbitrary yield scale of Fig. 3 are approximately 0.910, 0.939, and 1.03 when using the branching ratios of Ref. [3], Ref. [4], and of the present work, respectively. This represents a yield increase of 13% and 9.8% from Refs. [3, 4] to the present work. The changes in the yield are not exactly the same as the changes in branching ratios because of small (<1%) differences in f_{SC} for the 3 sets of branching ratios.

V. CONCLUSIONS

Data from the decay of the $E_r^{cm} = 458$ keV resonance in the ^{22}Ne(p,γ)^{23}Na reaction were analyzed using the TFractionFitter [8] class of ROOT [9]. New branching ratios have been derived, including a newly discovered branch to the 7082-keV state in ^{23}Na and a decrease of 10–13% in the ground-state branching ratio versus the results of Refs. [3] and [4]. We recommend a resonance strength of $\omega\gamma(458\text{ keV}) = 0.583(43)$ eV based on these results. This is different from the high-precision measurement of Longland et al. [6] by ∼1.2 σ and affects all higher-lying ^{22}Ne(p,γ)^{23}Na resonances. The uncertainty in the resonance strength has also been reduced from 9.7% [6] to 7.3%.

Appendix: Coincidence-Summing Correction Method Validation

The sum-correction method described in Sec. IV B is unique in that it provides a self-consistent method of coincidence-summing corrections. In practice, detector

total and full-energy peak efficiencies and Q solid angle attenuation coefficients are often required as external input in order to calculate the necessary coincidence-summing corrections (see Sec. IV B). With this method of sum correction all of these parameters are accounted for within the simulation, thereby eliminating the need for their external calculation. It is also interesting that an entire sum-corrected simulation spectrum is produced with this method. This spectrum could, in principle, be used to correct escape peaks for coincidence effects as well. Analysis of these peaks could provide further insight into characteristics of the detector being used. As this sum-correction method has never appeared in any published work to date, validation of this method is in order.

The effects of coincidence summing on experimental spectra decrease as the distance from the source to the detector is increased [19]. Thus, we chose to test the coincidence-summing correction method described in Sec. IV B with experimental data from the E_r^{cm} = 259 keV resonance in the ^{14}N(p,γ)^{15}O reaction at multiple source-to-detector distances. We validate this sum-correction method by displaying its ability to accurately sum correct data containing the varying levels of coincidence summing seen at each source-to-detector distance. The JN van de Graaff accelerator described in Sec. II provided a proton beam of $\sim$30 μA at an energy of 282$\pm$2 keV in the lab frame for this work. Data were collected with the 135% relative efficiency Ge detector described in Sec. II. A target of ^{14}N implanted at an energy of 40 keV into a tantalum target backing was used for data collection. The target was approximately 12 keV thick at the resonance energy.

The minimum possible source-to-detector distance is 1.1 cm for the experimental setup used here, as described in Refs. [10–12, 15]. Resonance decay spectra were collected with 0, 5, 10, and 20 cm added to this minimum source-to-detector distance and total beam charges of 0.064, 0.10, 0.26, and 0.40 C were accumulated at each distance, respectively. Simulations of each data set were calculated with GEANT, version 4.9.6, using the resonant state branching ratios of Marta et al. [39]. All γ-ray angular distributions and direction-direction correlations were calculated using the level spin assignments found in Ref. [40] according to the methods described in Ref. [19] and were included in every simulation. The agreement between experiment and simulation for data accumulated at each source-to-detector distance was similar to that of Fig. 1. Each simulation was fit to its respective experimental data set to derive N_R^{data} at each source-to-detector distance according to the method described in Sec. III.

The simulations were used to derive sum-correction factors for each primary and secondary photopeak observed in the data as detailed in Sec IV B. The full-energy peak efficiencies for each primary and secondary γ-ray at each distance were then calculated with [19]

$$\eta_p = \frac{N_\gamma f_{SC}}{BW N_R^{data}}. \quad \text{(A.1)}$$

Peak efficiencies derived from the data obtained with 0, 5, 10, and 20 cm added source-to-detector distance are shown from top to bottom in Fig. 4 using diamonds, squares, circles, and crosses, respectively. Data points that have been corrected for coincidence-summing effects are shown as the full, blue data points while the uncorrected data are shown as open, black data points. The expected full-energy peak efficiency curve for each source-to-detector distance was calculated using a series of mono-energetic γ-ray simulations, shown as dashed lines in Fig. 4. These expected peak efficiency curves have been scaled to include an independent, experimentally measured peak efficiency at 1333 keV, calculated using the sum-peak method [19] with ^{60}Co data taken at each source-to-detector distance. Although the resonant state transition to the 5241-keV state in ^{15}O was included in all simulations, it was not observed above background in every data set. Therefore, detector efficiencies were not calculated for γ-ray energies corresponding to that transition.

The uncorrected data points show evidence of coincidence-summing effects, especially with 0 cm added source-to-detector distance. This is most clearly seen in the ground-state transition data points at 7556 keV. However, the branching ratio for the ground-state transition from this resonance is $< 2\%$ [38, 39, 41]. The weakness of this branch coupled with the two-γ cascades that dominate the decay channels from this resonance enhance the effect of coincidence summing for this data point at 0 cm added distance such that up to $\sim$80% of the ground-state transition photopeak is a result of summing-in.

Another way to look at this situation is by considering the relative probability of capturing the full energy of both γ-rays of a two-γ cascade relative to that of capturing the full energy of the ground-state transition γ-ray. At 0 cm added source-to-detector distance, the probability of detecting the sum energy of the R$\rightarrow$6176$\rightarrow$0 cascade is $\sim$5.2% of that for detecting the full energy of the ground-state transition. In other words, if there were an equal number of ground-state and R$\rightarrow$6176$\rightarrow$0 decays with no other possibility for decay from the resonant state, then $\sim$5.2% of the ground state transition peak would be be the result of summing-in. This relative probability drops to only $\sim$0.3% at 20 cm added distance. However, since the R$\rightarrow$6176$\rightarrow$0 cascade is actually about 40 times as likely as the ground state transition, summing-in is significant even at 20 cm.

It is important to note that coincidence summing was indeed observed in the data taken with 20 cm added source-to-detector distance. This is of importance for the primary branching ratios from this resonance in ^{14}N(p,γ)^{15}O reported in Runkle et al. [41] and Imbriani et al. [38]. The same HPGe detector used in this work was also used in Ref. [41]. A source-to-detector distance of

23 cm was used for branching ratio measurements in that work under the assumption that there was no coincidence summing present in the accumulated data. Given that we observe coincidence summing with the detector at 21.1 cm, it is likely that coincidence summing was, in fact, present in that data. A 126% relative efficiency HPGe detector was used in Ref. [38] with source-to-detector distances ranging from 1.5 to 20.5 cm. Their branching ratios were determined from a fit to each of four data sets at varying source-to-detector distances, leaving the branching ratios themselves as free parameters of the fit. However, given that the ground state branching ratio reported in Ref. [38] is ∼15% greater than that reported in Marta et al. [39], coincidence summing may have had an effect on the results of Ref. [38]. Here we assume the branching ratios of Marta et al. [39] are free of coincidence-summing effects.

Agreement within uncertainty is, in general, achieved between the expected efficiency curves at each distance and the sum-corrected peak efficiency data points for the same distance. This implies that these data were accurately corrected for coincidence-summing effects, thereby validating this sum-correction method.

ACKNOWLEDGMENTS

The authors would like to acknowledge instructive assistance from C. Howard, J.R. Dermigny, and C. Iliadis during the writing and data analysis process. The authors would also like to thank the referee for insightful suggestions to improve the clarity of this paper. This work was supported by the US Department of Energy under grant DE-FG02-97ER41041.

[1] R. B. Firestone, Nucl. Data Sheets **108**, 1 (2007).
[2] J. M. Cesaratto, A. E. Champagne, M. Q. Buckner, T. B. Clegg, S. Daigle, C. Howard, C. Iliadis, R. Longland, J. R. Newton, and B. M. Oginni, Phys. Rev. C **88**, 065806 (2013).
[3] M. Piiparinen, A. Anttila, and M. Viitasalo, Z. Phys. **247**, 400 (1971).
[4] M. A. Meyer and J. J. A. Smit, Nucl. Phys. A **205**, 177 (1973).
[5] P. M. Endt, Nucl. Phys. A **633**, 1 (1998).
[6] R. Longland, C. Iliadis, J. M. Cesaratto, A. E. Champagne, S. Daigle, J. R. Newton, and R. Fitzgerald, Phys. Rev. C **81**, 055804 (2010).
[7] S. Agostinelli, J. Allison, K. Amako, J. Apostolakis, H. Araujo, and P. Arce, Nucl. Instrum. and Methods A **506**, 250 (2003).
[8] R. Barlow and C. Beeston, Comp. Phys. Commun. **77**, 219 (1993).
[9] R. Brun and F. Rademakers, Nucl. Instrum. Methods A **81**, 389 (1997).
[10] J. M. Cesaratto, A. E. Champagne, T. B. Clegg, M. Q. Buckner, R. C. Runkle, and A. Stefan, Nucl. Instrum. and Methods A **623**, 888 (2010).
[11] R. Longland, C. Iliadis, A. E. Champagne, C. Fox, and J. R. Newton, Nucl. Instrum. and Methods A **566**, 452 (2006).
[12] M. Q. Buckner, C. Iliadis, J. M. Cesaratto, C. Howard, T. B. Clegg, A. E. Champagne, and S. Daigle, Phys. Rev. C **86**, 065804 (2012).
[13] C. Howard, C. Iliadis, and A. E. Champagne, Nucl. Instrum. and Methods A **729**, 254 (2013).
[14] S. Carson, C. Iliadis, J. M. Cesaratto, A. E. Champagne, L. N. Downen, M. Ivanovic, J. Kelley, R. Longland, J. R. Newton, G. Rusev, and A. P. Tonchev, Nucl. Instrum. Methods A **618**, 190 (2010).
[15] M. Q. Buckner, C. Iliadis, K. J. Kelly, L. N. Downen, A. E. Champagne, J. M. Cesaratto, C. Howard, and R. Longland, Phys. Rev. C **91**, 015812 (2015).
[16] M. Q. Buckner, Ph.D. thesis, University of North Carolina at Chapel Hill (2015).
[17] S. Daigle, Ph.D. thesis, University of North Carolina at Chapel Hill (2014).
[18] J. Dermigny *et al.*, Nucl. Instrum. and Methods A , to appear.
[19] C. Iliadis, *Nuclear Physics of Stars* (Wiley-VCH Verlag GmbH and Co. KGaA Weinheim, 2007).
[20] F. James and M. Roos, CERN Program Library **D506** (1988).
[21] G. Knoll, *Radiation Detection and Measurements* (John Wiley and Sons, 1996).
[22] M.-C. Lépy, T. Altzitzoglou, M. J. Anagnostakis, D. Arnold, M. Capogni, and A. Ceccatelli, Appl. Radiat. Isotopes **68**, 1407 (2010).
[23] F. Piton, M.-M. Lépy, M.-C. Bé, and J. Plagnard, Appl. Radiat. Isotopes **52**, 791 (2000).
[24] M.-C. Lépy, P. Brun, C. Collin, and J. Plagnard, Appl. Radiat. Isotopes **64**, 1340 (2006).
[25] O. Sima and D. Arnold, Appl. Radiat. Isotopes **53**, 51 (2000).
[26] O. Sima and D. Arnold, Appl. Radiat. Isotopes **64**, 64 (2006).
[27] O. Sima and D. Arnold, Appl. Radiat. Isotopes **66**, 705 (2008).
[28] M. Debertin and U. Schötzig, Nucl. Instrum, Methods A **158**, 471 (1979).
[29] K. Sinkko and H. Aaltonen, (In: Finnish Centre for Radiation and Nuclear Safety, Surveillance Department, STUK-B-VALO 40, Helsinki, 1985).
[30] S. Sudár, IAEA Tecdoc **1275**, 37 (2002).
[31] G. Kanisch, T. Vidmar, and O. Sima, Appl. Radiat. Isotopes **67**, 1952 (2009).
[32] P. De Felice, P. Angelini, A. Fazio, and R. Biagini, Appl. Radiat. Isotopes **52**, 745 (2000).
[33] S. Hurtado, M. Garcia-Leon, and R. Garcia-Tenorio, Appl. Radiat. Isotopes **52**, 745 (2000).
[34] S. Hurtado, R. Garcia-Tenorio, and M. Garcia-Leon, Appl. Radiat. Isotopes **52**, 745 (2000).
[35] T. M. Semkow, G. Mehmood, P. P. Parekh, and M. Virgil, Nucl. Instrum. and Methods A **A290**, 437 (1990).
[36] R. C. Runkle, A. E. Champagne, C. Fox, C. Iliadis, J. Pollanen, A. Stephan, and C. Westerfeldt, Phys. Rev. C. **66**, 022801(R) (2002).

[37] A. Formicola, G. Imbriani, H. Costantini, C. Angulo, and D. Bemmerer, Phys. Lett. B **591**, 61 (2004).
[38] G. Imbriani, H. Costantini, A. Formicola, A. Vomiero, C. Angulo, and D. Bemmerer, Eur. Phys. J. A **25**, 455 (2005).
[39] M. Marta, A. Formicola, D. Bemmerer, C. Broggini, A. Caciolli, P. Corvisiero, H. Costantini, Z. Elekes, *et al.*, Phys. Rev. C **83**, 045804 (2011).
[40] F. Ajzenberg-Selove, Nucl. Phys. A **523**, 1 (1991).
[41] R. C. Runkle, A. E. Champagne, C. Angulo, C. Fox, C. Iliadis, R. Longland, and J. Pollanen, Phys. Rev. Lett. **94**, 082503 (2005).

FIGURES

FIG. 1. (color online) The result of the best fit, shown in green, to experimental data on the 458-keV resonance in the ^{22}Ne(p,γ)^{23}Na reaction, shown in black, as derived using the TFractionFitter [8] class of ROOT [9] and the methodology detailed in the text and in Ref. [15]. Resonance primary peaks are indicated by blue arrows. The fit was derived considering GEANT [7] simulations of each potential decay cascade from the $J_R = 1/2$ 9252-keV resonant state in ^{23}Na excited by this resonance to all lower lying states with $J = 1/2$, 3/2, or 5/2. Only those with nonzero contributions were kept for the fit shown here. The two highest branching ratio templates are shown in blue with the room background spectrum shown in red. A total of eight other decay cascade templates were used for the fit shown here. Branching ratios were derived using the relative contributions of these simulations and are shown in Tab. I.

FIG. 2. (color online) The experimental yield from the E_r^{cm} = 458 keV resonance from the 6270 and 2170-keV γ-rays observed in this work, shown as black circles and red diamonds, respectively. The yield scale for data points of either color is given by the y-axis of the same color. The 2170-keV γ-ray corresponds to a new primary transition, first identified in this work, to the 7082-keV state in ^{23}Na while the 6270-keV γ-ray corresponds to the well-known R→2982 transition. Definitive identification of the 2170-keV γ-ray as a resonant state decay in ^{23}Na is provided by the similarity between the measured yield of these two γ-rays.

FIG. 3. (color online) A plot of Y_j, the experimental yield from the E_r^{cm} = 458 keV resonance in the ^{22}Ne(p,γ)^{23}Na reaction, for all primary γ-ray transition peaks. The Y_j values calculated using the branching ratios of Piiparinen et al. [3] are shown as red squares, those using Meyer et al. [4] are shown as open circles, and those using the present branching ratios are shown as blue diamonds. The dashed line at Y_j=1 is shown to help guide the eye, while the dashed lines above and below Y_j=1 represent a factor of 2 and 3 deviation from Y_j=1. The geometric standard deviation, σ^{geo}, of each data set is shown as well. See text for a discussion of the data shown here.

FIG. 4. (color online) Full-energy peak efficiencies of the 135% HPGe detector used in this work derived from data on the E_r^{cm} = 259 keV resonance in the ^{14}N(p,γ)^{15}O reaction. Data were taken with 0, 5, 10, and 20 cm added to the minimum source-to-detector distance of 1.1 cm, shown above as the diamond, square, circle, and cross data points, respectively. Data that were sum corrected (SC) and data that were not sum corrected (NSC) are shown as full, blue and open, black data points, respectively. Dashed lines represent the expected full-energy peak efficiency curve of the HPGe detector at each source-to-detector distance, each of which have been scaled to include an independent, experimental peak efficiency measurement at 1333 keV. In general, agreement is achieved between the sum-corrected data and the expected peak efficiency curve at each distance.

TABLES

TABLE I. Branching ratios for primary transitions (in %) from the 458-keV resonance in the ^{22}Ne(p,γ)^{23}Na reaction. Note that the R→3848 transition was not observed in the present work. See the text for details.

Transition	Present Work	Ref. [4]	Ref. [3]
R→0	41.77(67)	46.0	48.0
R→2391	4.05(12)	3.7	5.0
R→2640	8.27(18)	8.5	6.0
R→2982	31.73(52)	32.0	39.0
R→3678	4.85(16)	4.1	-
R→3848	-	-	2.0
R→3914	0.37(9)	0.7	-
R→4430	1.69(9)	1.8	-
R→5766	2.78(9)	2.4	-
R→6921	2.43(9)	0.8	-
R→7082	2.06(9)	-	-

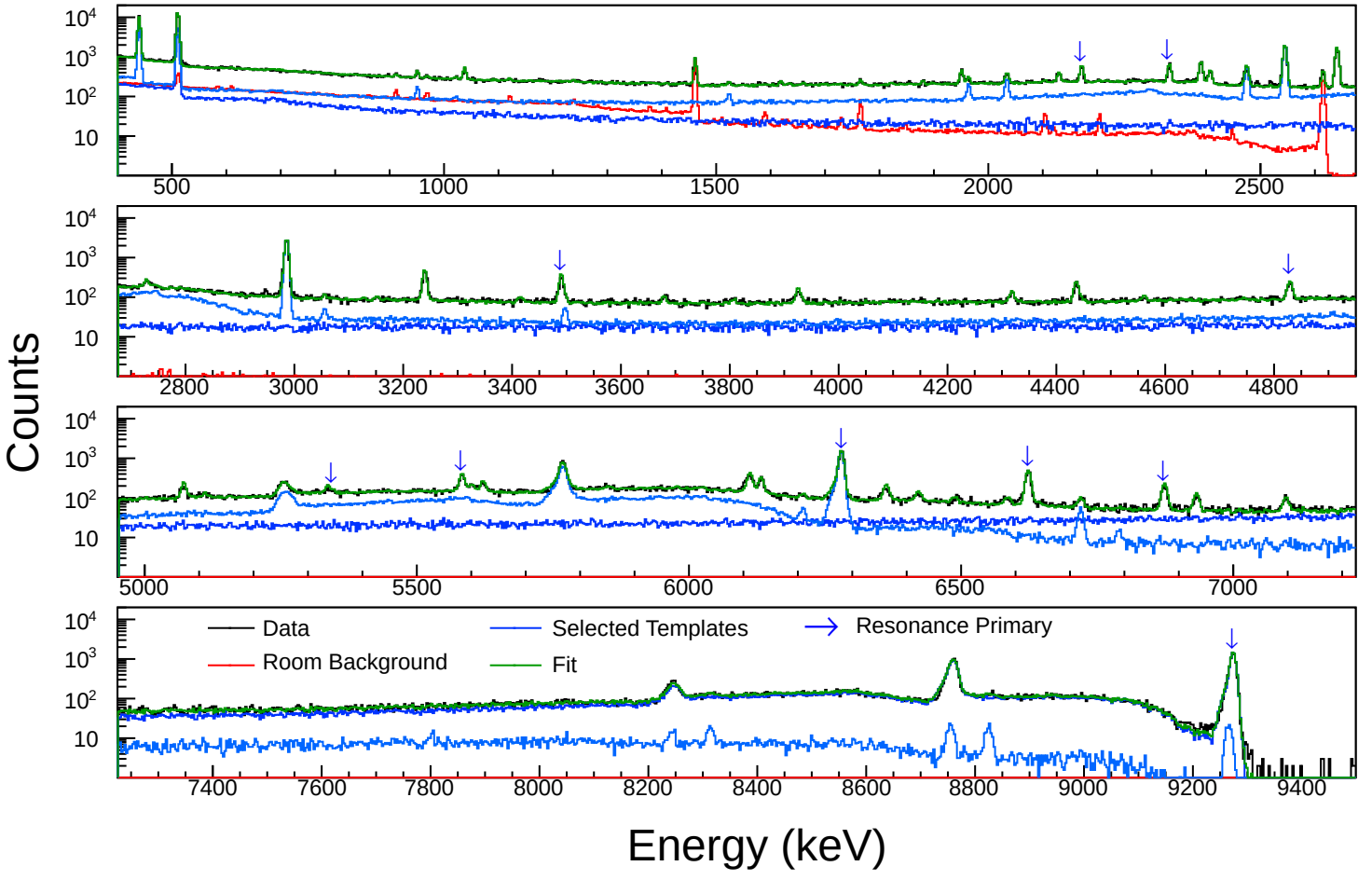
Counts
Energy (keV)
Data
Room Background
Selected Templates
Fit
Resonance Primary

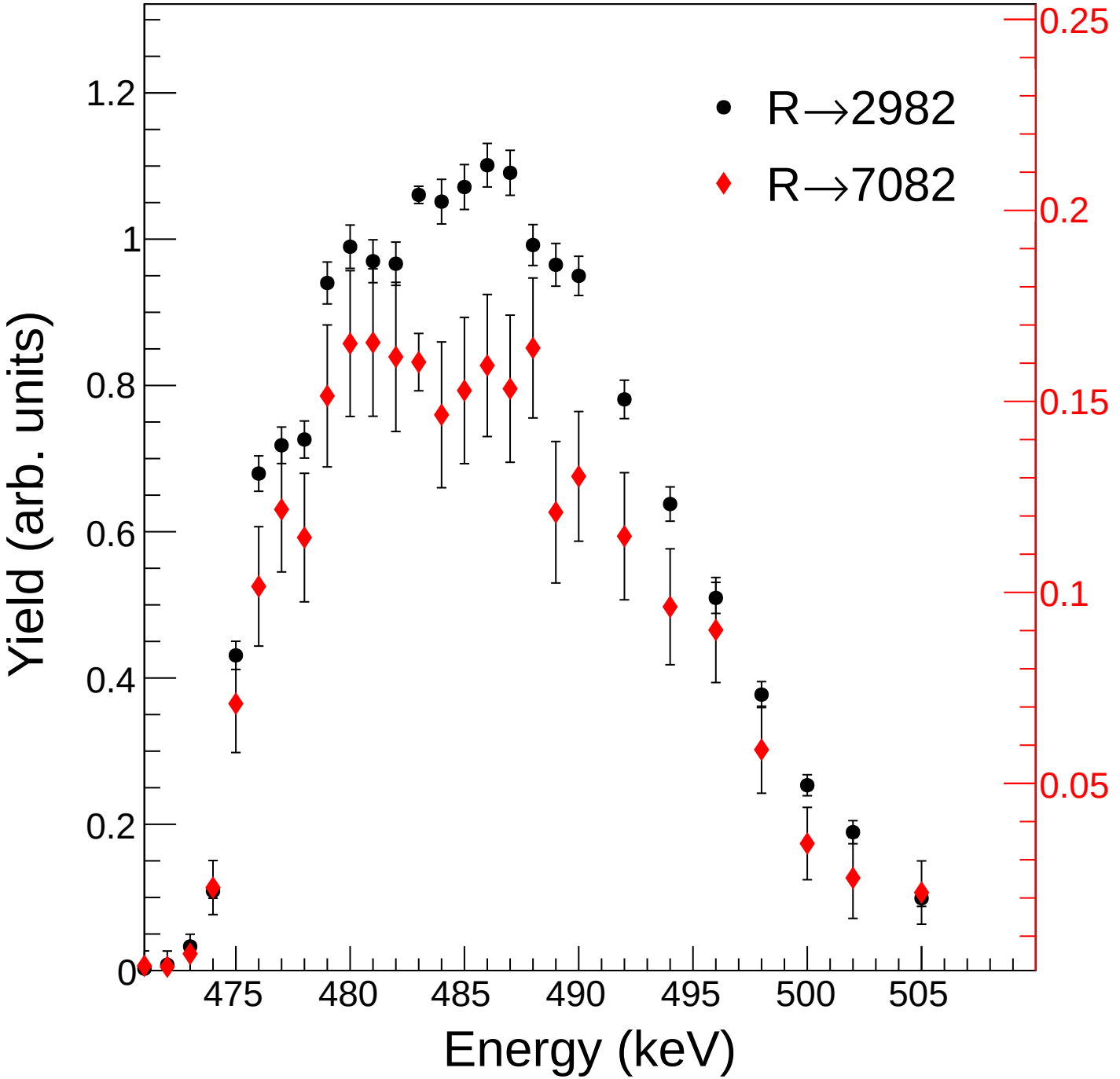
R→2982
R→7082
Yield (arb. units)
Energy (keV)
0
0.2
0.4
0.6
0.8
1
1.2
0.05
0.1
0.15
0.2
0.25
475
480
485
490
495
500
505

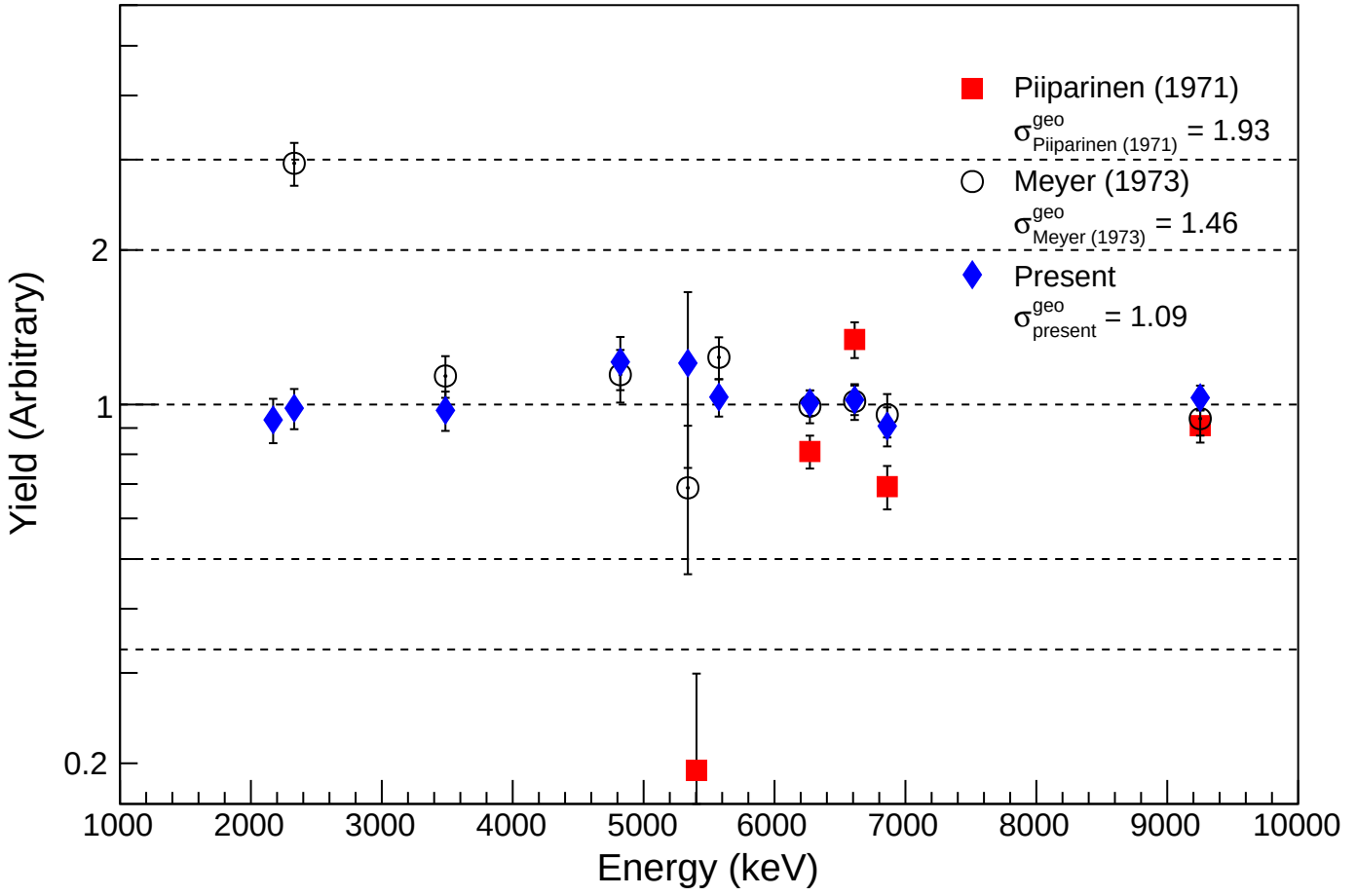
Piiparinen (1971)
$\sigma^{geo}_{Piiparinen\ (1971)}$ = 1.93
Meyer (1973)
$\sigma^{geo}_{Meyer\ (1973)}$ = 1.46
Present
$\sigma^{geo}_{present}$ = 1.09
Yield (Arbitrary)
2
1
0.2
1000
2000
3000
4000
5000
6000
7000
8000
9000
10000
Energy (keV)

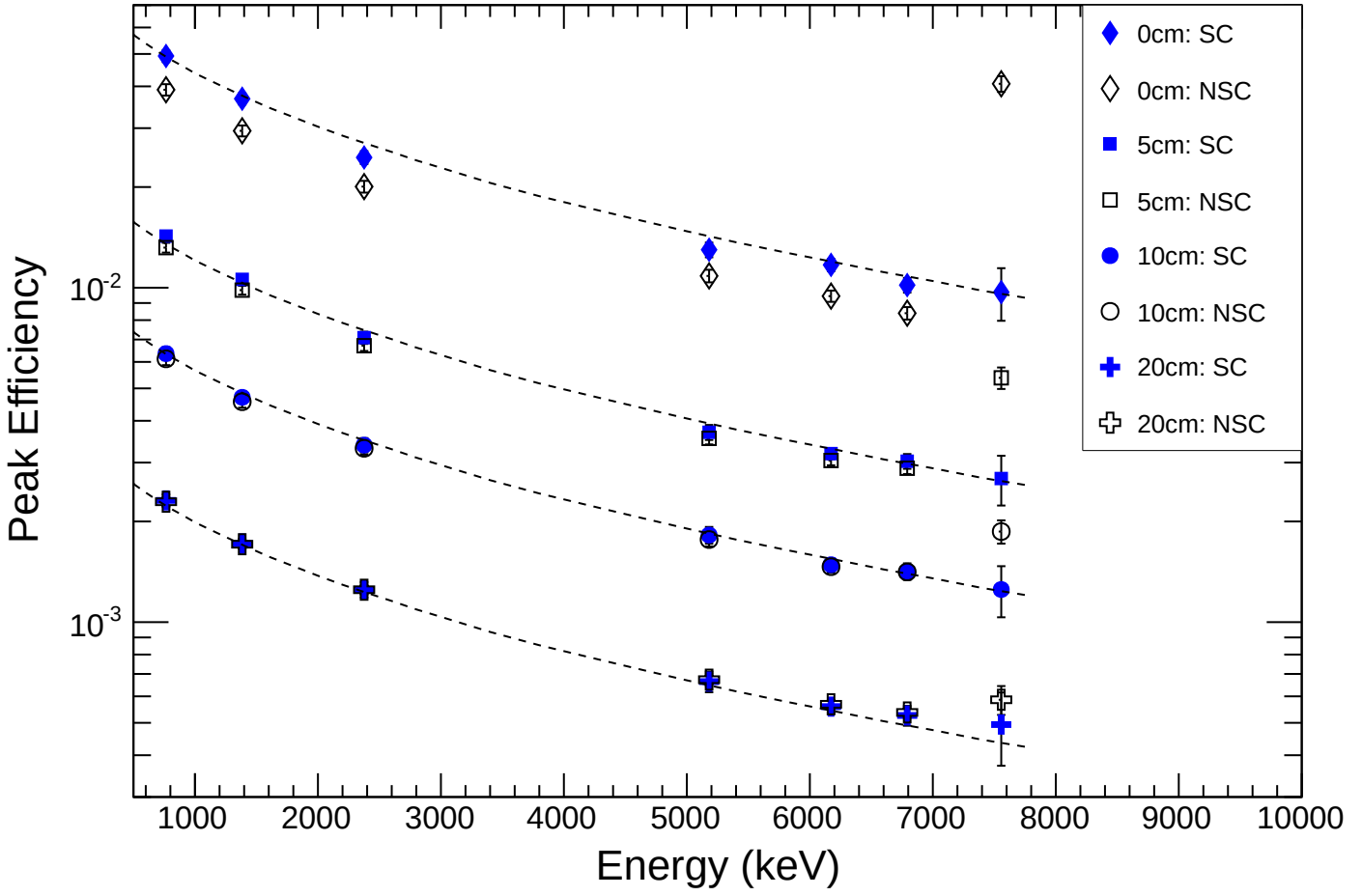
Peak Efficiency
10^{-2}
10^{-3}
1000
2000
3000
4000
5000
6000
7000
8000
9000
10000
Energy (keV)
0cm: SC
0cm: NSC
5cm: SC
5cm: NSC
10cm: SC
10cm: NSC
20cm: SC
20cm: NSC